

Stabilization of Multi-Group Neutron Transport with Transport-Corrected Cross-Sections

Geoffrey Gunow^a, Benoit Forget^b, Kord Smith^b

^aBloomberg LP 731 Lexington Avenue, New York, NY 10022, United States

^bMassachusetts Institute of Technology, Department of Nuclear Science and Engineering, 77 Massachusetts Avenue, Building 24, Cambridge, MA 02139, United States

Abstract

Many deterministic neutron transport solvers rely on the source iteration method to solve the multi-group neutron transport equation. Often, these solvers rely on transport corrected cross-sections for accurate prediction of the neutron flux distribution. Transport corrected within-group scattering cross-sections can become negative, and if these negative cross-sections are large in magnitude, source iteration can become unstable and fail to converge for certain cases. In this study, we present evidence of this convergence issue for the Method of Characteristics (MOC) on full-core PWR problems with common transport correction schemes. A theoretical discussion is presented to illustrate the reason for the convergence issues. Previously established stabilization methods are compared with a newly proposed stabilization method. Results show that the new stabilization method allows for faster convergence than previous techniques. In addition, the effect of Coarse Mesh Finite Difference (CMFD) acceleration on stability is analyzed, showing that CMFD acceleration with full-group structure can overcome the convergence issues, but a stabilization technique is necessary for convergence when a condensed group structure is used.

Keywords: Transport Correction, Convergence, Neutron Transport, Method of Characteristics

1. Introduction

In order to capture the effect of anisotropic scattering, multi-group deterministic transport solvers can either directly account for anisotropic scattering using high order scattering approximations or can use a transport correction to the multi-group cross-sections Bell et al. (1967). Many solvers use the transport correction to avoid the increased computational complexity from directly accounting for anisotropic scattering. While many forms of the transport correction have been developed MacFarlane (1993, 2000); HÉbert (2009), all notable formulations replace the total cross-section with a transport cross-section, which is smaller in magnitude to account for increased propagation of neutrons along the direction of travel, while adjusting within-group scattering to preserve balance. Specifically, for a region i and energy group g , the transport correction $\Delta\Sigma_{tr}^{i,g}$ is applied to both the total cross-section $\Sigma_t^{i,g}$ and within-group scattering cross-section $\Sigma_s^{i,g \rightarrow g}$ resulting in a transport cross-section $\Sigma_{tr}^{i,g}$ and transport-corrected within-group scattering cross-section $\tilde{\Sigma}_{s,i}^{g \rightarrow g}$ as:

$$\begin{aligned}\Sigma_{tr}^{i,g} &= \Sigma_t^{i,g} - \Delta\Sigma_{tr}^{i,g} \\ \tilde{\Sigma}_s^{i,g \rightarrow g} &= \Sigma_s^{i,g \rightarrow g} - \Delta\Sigma_{tr}^{i,g}\end{aligned}\quad (1)$$

For notational convenience, the remainder of this study will refer to $\tilde{\Sigma}_s^{i,g \rightarrow g}$ as being the transport corrected $\tilde{\Sigma}_s^{i,g \rightarrow g}$ when transport correction is applied.

When using a cross-section set with a large number of energy groups, the within-group scattering cross-sections can be small. When transport correction is then applied, the correction can be greater than the within-group scattering cross-section, resulting in negative modified within-group scattering cross-sections. Tabuchi discovered negative within-group scattering cross-sections to be an issue when converging within-group scattering iterations Tabuchi et al. (2013) in the method of characteristics (MOC). Specifically, it was identified that the within-group scattering matrix could have a spectral radius greater than unity, causing the system not to converge. Tabuchi later proposed a stabilization technique for inner iterations Tabuchi et al. (2014).

This study expands upon the ideas presented by Tabuchi to explain the observed convergence behavior of source iteration without inner iterations. OpenMOC, an open-source MOC solver W. Boyd, S. Shaner, L. Li, B. Forget, and K. Smith (2014), is used to analyze convergence behavior of transport methods with transport corrected cross-sections. Realistic full core cases are presented that observe the failed convergence behavior and a new stabilizing method is proposed that stabilizes source iteration. This analysis focuses on a flat source approximation, though the stabilization technique has shown to also stabilize linear source MOC Gunow (2018).

2. Theory

2.1. Matrix Representation of the Transport Equation

The multi-group transport equation can be solved by a variety of methods including MOC and Discrete Ordinates

Email addresses: geogunow@mit.edu (Geoffrey Gunow), bforget@mit.edu (Benoit Forget), kord@mit.edu (Kord Smith)

(S_N) . This study concentrates on methods with an isotropic scattering assumption. Many of these methods discretize the transport equation in some fashion and solve a linear system of the form

$$\boldsymbol{\phi} = J \left(\frac{1}{k} F + S \right) \boldsymbol{\phi} \quad (2)$$

where $\boldsymbol{\phi}$ represents the vector of all scalar fluxes, J is the transport sweep matrix, F is the fission matrix, S is the scattering matrix, and k is the eigenvalue. In many efficient transport solvers, these matrices are not explicitly formed but rather they implicitly solve these equations with sweeps taking the place of explicit matrix-vector multiplications. Therefore, these matrices are often presented as operators rather than matrices, but the underlying matrix elements could be computed if desired [Gunow \(2018\)](#). Specifically, the matrices F and S are defined by

$$F_{(i,g),(i,g')} = \frac{1}{4\pi} \chi_{i,g} \nu \Sigma_f^{i,g'} \quad (3)$$

and

$$S_{(i,g),(i,g')} = \frac{1}{4\pi} \Sigma_s^{i,g' \rightarrow g} \quad (4)$$

with rows and columns indexed by (i, g) where i is the region and g is the energy group. (For instance, the matrix index could be computed as $i \times G + g$ where G is the number of energy groups.) All unspecified matrix elements are zero. The transport sweep matrix J has a much more complicated form and is dependent on the specific transport approximations. Matrix-vector products with J are often termed *transport sweeps*.

2.2. Equivalence with Collision Probability Methods

While deterministic methods with a flat source approximation can have different structures for the matrix J , they all solve the same physical system. Therefore, as the discretization is refined, the matrix J becomes equivalent across methods, only differing in the way matrix-vector products with J are computed. The MOC method used in this study is equivalent to the collision probability form as discretization is refined [Tabuchi et al. \(2013\)](#). Although collision probabilities do not explicitly enter the MOC equations, the neutron balance equation takes the form in Eq. 5:

$$\Sigma_{tr}^{i,g} \phi_{i,g} V_i = \sum_j P_{ji,g} q_{j,g} V_j \quad (5)$$

where $P_{ji,g}$ represents the probability of a neutron of energy group g going from region j and having a collision in region i , V_i represents the volume of region i , $q_{i,g}$ represents the neutron source and $\phi_{i,g}$ represents the average scalar flux in region i and group g . In general, the neutron source can be computed by summing contributions from all G energy groups as

$$q_{i,g} = \sum_{g'=1}^G \left(\Sigma_s^{i,g' \rightarrow g} \phi_{i,g'} + \chi_{i,g} \nu \Sigma_f^{i,g'} \phi_{i,g'} \right) \quad (6)$$

where $\Sigma_s^{i,g' \rightarrow g}$ is the scattering cross-section in region i from group g' to group g , $\chi_{i,g}$ is the fission emission probability for group g in region i , and $\nu \Sigma_f^{i,g'}$ is the fission production in region i from group g' . Combining this definition with Eq. 5, as well as the reciprocity relationship,

$$P_{ij,g} \Sigma_{tr}^{i,g} V_i = P_{ji,g} \Sigma_{tr}^{j,g} V_j, \quad (7)$$

neutron balance can be presented in the form of Eq. 8.

$$\phi_{i,g} = \sum_j \frac{P_{ij,g} \sum_{g'=1}^G \left(\Sigma_s^{j,g' \rightarrow g} \phi_{j,g'} + \chi_{j,g} \nu \Sigma_f^{j,g'} \phi_{j,g'} \right)}{\Sigma_{tr}^{j,g}} \quad (8)$$

Notice that this is in the form of Eq. 2. Therefore, the matrix $A = J \left(\frac{1}{k} F + S \right)$ can be expressed as

$$A_{(i,g),(j,g')} = P_{ij}^g \left(\frac{\chi_{j,g} \nu \Sigma_f^{j,g'}/k + \Sigma_s^{j,g' \rightarrow g}}{\Sigma_{tr}^{j,g}} \right). \quad (9)$$

Note that matrix A is square and dense with length equal to the number of scalar fluxes.

2.3. Iteration Schemes

2.3.1. Power Method

One method to solve a system of the form given in Eq. 2 is the power method, which yields the dominant eigenvector corresponding to the steady-state flux distribution. To invoke the power method [Hansen \(1964\)](#), Eq. 2 can be re-arranged to the form in Eq. 10 where I represents the identity matrix.

$$\begin{aligned} Z &\equiv (I - JS)^{-1} J F \\ Z \boldsymbol{\phi} &= k \boldsymbol{\phi} \end{aligned} \quad (10)$$

With the power method scheme, repeated multiplication by Z yields the dominant eigenvector [Bradie \(2006\)](#). Rather than performing strict power method iterations, the estimate of the eigenvalue k_n at iteration n is often included in the source. This scheme is presented in Eq. 11. These iterations are often termed *outer iterations*.

$$\boldsymbol{\phi}_{n+1} = (I - JS)^{-1} J \frac{F}{k_n} \boldsymbol{\phi}_n \quad (11)$$

Since explicitly taking the matrix inverse of $I - JS$ is unwise, an iterative scheme is necessary to solve the linear system. In many transport methods, such as MOC, computing the elements of J can be as expensive as computing a matrix-vector product [Gunow \(2018\)](#). In addition, recall that each matrix-vector product with matrix J is usually quite expensive. Therefore, few methods are available to efficiently solve the linear system in practice. This leads to solving the equation at *inner iteration* m with the scheme illustrated in Eq. 12. The scalar flux $\boldsymbol{\phi}_{n,0}$ refers to the scalar flux at the start of the inner iterations whereas $\boldsymbol{\phi}_{n,m}$ refers to the scalar flux at inner iteration m .

$$\boldsymbol{\phi}_{n,m+1} = J \left(\frac{1}{k_n} F \boldsymbol{\phi}_{n,0} + S \boldsymbol{\phi}_{n,m} \right) \quad (12)$$

It is important to note that iterative schemes such as this require that the iteration matrix, in this case JS , have a spectral radius less than unity [Bradie \(2006\)](#). Here, the full scattering source is updated at every iteration. However, it is more common to only update the within-group scattering source, as described in Eq. [13](#)

$$\boldsymbol{\phi}_{n,m+1} = J \left(\left(\frac{1}{k_n} F + S_{out} \right) \boldsymbol{\phi}_{n,0} + S_{in} \boldsymbol{\phi}_{n,m} \right) \quad (13)$$

where $S = S_{in} + S_{out}$. S_{in} is the diagonal elements of S referring to within-group scattering and S_{out} is the off-diagonal elements. In this scheme, the iteration matrix is JS_{in} rather than JS .

2.3.2. Source Iteration without Inner Iterations

An alternative way to solve the transport equation is to directly apply the transport sweep to the full neutron source. Note that the neutron source \mathbf{q} can be computed as

$$\mathbf{q} = \left(\frac{1}{k} F + S \right) \boldsymbol{\phi}.$$

The transport sweep matrix J therefore yields the scalar flux distribution associated with the computed source distribution. In this form, a new iterative process could be introduced in which a new source distribution is computed at each iteration, yielding a new estimate of the associated scalar flux distribution. Therefore, solving the transport equation in this form where source terms are lagged is termed *source iteration*. Specifically, the eigenvalue problem in Eq. [2](#) is iteratively solved with the left hand side updated and the right hand side lagged as

$$\boldsymbol{\phi}_{n+1} = J \left(\frac{F \boldsymbol{\phi}_n}{k_n} + S \boldsymbol{\phi}_n \right). \quad (14)$$

It is important to note that this process is non-linear due to the iteration matrix $J \left(\frac{1}{k_n} F + S \right)$ being dependent on the iteration number n . To simplify this relationship, assume that the eigenvalue k is perfectly known to be k_{crit} , the eigenvalue associated with the dominant mode of the system. In reality, the exact value of k_{crit} is not known *a priori* but observations and intuition suggests that it does not strongly impact convergence. With the eigenvalue fixed, the system becomes

$$\boldsymbol{\phi}_{n+1} = A \boldsymbol{\phi}_n \quad (15)$$

where matrix A is defined in Eq. [9](#) with $k = k_{crit}$. This process is equivalent to the power method iterations with the matrix A , which converges to the eigenvector associated with the dominant eigenvalue of A . Since k_{crit} is the dominant eigenvalue of the original system, 1.0 must be an eigenvalue of A . In addition, if an everywhere positive solution exists, it must be associated with the physical solution.

Recall from Eq. [9](#) that the iteration matrix A is everywhere positive and real as long as the within-group scattering cross-section is positive. According to the Perron-Frobenius Theorem [Graham \(1987\)](#), square matrices of all positive real

entries have a unique largest real eigenvalue which is dominant and associated with an everywhere positive eigenvector. In addition, all other eigenvectors must have a negative component. Without transport correction, the iteration matrix A is an all positive and real matrix, implying that the largest eigenvalue is 1.0 and is associated with the physical solution. Therefore, the process detailed in Eq. [14](#) will converge to the physical solution.

However, with the transport correction, it is possible to have negative within-group scattering, causing this condition not to hold. Therefore, the system might still converge, but convergence cannot be guaranteed under the Perron-Frobenius Theorem. Therefore, the iteration scheme should be updated to ensure convergence.

3. Stabilization of Source Iteration

Note that Eq. [16](#) is a mathematically valid rewriting of Eq. [2](#) for any matrix D where $I + D$ is invertible.

$$\boldsymbol{\phi} = (I + D)^{-1} \left[J \left(\frac{1}{k} F + S \right) + D \right] \boldsymbol{\phi} \quad (16)$$

Next, the same source iteration scheme is applied where the left hand side is updated with the right hand side constant. Since $I + D$ needs to be easily invertible for this new scheme to be efficient, D is chosen to be diagonal. The convergence discussion then follows the same discussion as before except the new iteration matrix now has the form $\tilde{A} = (I + D)^{-1} \left[J \left(\frac{1}{k_{crit}} F + S \right) + D \right]$ with the matrix \tilde{A} is described by

$$\begin{aligned} \tilde{A}_{(i,g),(j,g')} &= \left[\frac{1}{1 + D_{(i,g),(i,g)}} \right] \times \\ &\left[P_{ij}^g \left(\frac{\chi_{j,g} \nu \Sigma_f^{j,g'} / k_{crit} + \Sigma_s^{j,g' \rightarrow g}}{\Sigma_{tr}^{j,g}} \right) + D_{(i,g),(j,g')} \right] \end{aligned} \quad (17)$$

where the rows and columns are again indexed by region, energy group pairs. The diagonal elements of D are chosen to be:

$$D_{(i,g),(i,g)} = \begin{cases} \frac{-\rho \Sigma_s^{i,g \rightarrow g}}{\Sigma_{tr}^{i,g}}, & \text{for } \Sigma_s^{i,g \rightarrow g} < 0 \\ 0, & \text{otherwise} \end{cases} \quad (18)$$

where the damping coefficient ρ is a positive value chosen by the user. For $\rho = 1$, the diagonal update ensures that there are no negative diagonal elements in the iteration matrix.

The diagonal stabilization scheme has the effect of shifting the iteration matrix eigenvalues to be more positive. The intuition for this shift is due to the Gershgorin Disk Theorem where eigenvalues exist in disks around diagonal elements of the matrix. Since the diagonal elements are increased and all matrix elements are contracted, the Gershgorin Disks are likewise shifted positive with their radii contracted. While

this improves stability, it also tightens the positive-eigenvalue modes, causing larger dominance ratios in the iteration matrix, and slower convergence. Therefore, ρ should be chosen to be small while still ensuring convergence. An illustration of the shift in eigenvalues is shown in Figure 1.

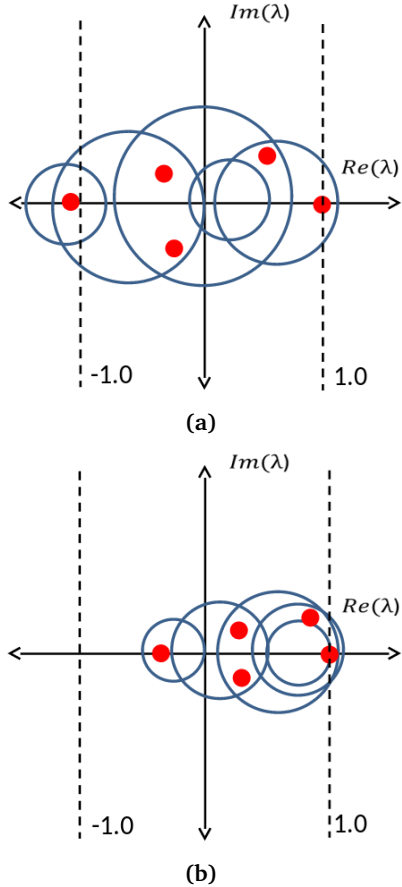


Figure 1. An illustration of diagonal dominance shifting the eigenvalues λ of a matrix with initial Gershgorin disks (blue) and eigenvalues (red) in the complex plane (a) shifted positively with diagonal stabilization (b). Note that the eigenvalue at 1.0 stays at 1.0.

Tabuchi suggested a similar scheme for converging within-group scattering iterations of MOC transport sweeps Tabuchi et al. (2014). Though originally limited to MOC transport sweeps with within-group scattering iterations, Tabuchi's scheme is equivalent to the diagonal stabilization scheme presented here for damping the scalar flux update except for the choice of diagonal matrix \tilde{D} in place of D with elements

$$\tilde{D}_{(i,g),(i,g)} = \max_j \left| \frac{\Sigma_s^{j,g \rightarrow g}}{\Sigma_{tr}^{j,g}} \right| \quad (19)$$

which is far larger than the equivalent formulation given in Eq. 18. Not only is the damping applied to all fluxes, not just those with negative within-group scattering, but it also takes the maximum ratio of within-group scattering to transport cross-section $\Sigma_s^{j,g \rightarrow g} / \Sigma_{tr}^{j,g}$ across all regions j , which may already be positive.

4. Implementation

4.1. OpenMOC

Recently OpenMOC Boyd et al. (2016), an open-source neutron transport code developed at MIT, has been extended to support direct 3D MOC calculations. It has been demonstrated to accurately and efficiently simulate the 3D full core BEAVRS benchmark Horelik et al. (2013), representing a realistic PWR core. This was accomplished by using an efficient track laydown Shaner et al. (2015), axially extruded ray tracing Gunow et al. (2016), a 3D linear source approximation Ferrer et al. (2012); Ferrer and Rhodes (1981); Gunow (2018), and efficient spatial domain decomposition Gunow (2018).

In order to test the convergence behavior of the stabilization methods, the previously discussed stabilization methods were implemented in OpenMOC. Leveraging the computational ability of OpenMOC to solve realistic full core 3D models, it is possible to observe convergence behavior on these very large and relevant problems. It should be noted that the implementation of the stabilization techniques is quite simple, requiring very little change in the existing code. The largest change is incorporating a second scalar flux vector for the previous iteration solution. The change should also be simple to implement in other neutron transport solvers.

It is important to note that in the OpenMOC implementation, negative sources are set to zero in the first 20 iterations. In addition, negative scalar fluxes are always set to zero. Whenever the correction is applied during an iteration, a warning message is displayed, alerting the user to the behavior. Negative sources and fluxes are an important indicator of convergence issues, as a solution corresponding with a negative eigenvalue will have negative components in its associated eigenvector. While setting negative sources and fluxes to zero helps the convergence behavior by more quickly eliminating non-physical behavior, it does not remedy the fundamental convergence issues introduced by negative cross-sections without the use of a stabilization technique such as diagonal stabilization.

4.2. Convergence Metrics

In order to determine convergence, this study monitors the fission neutron production rates. Specifically, the neutron production rate f_i in a source region i can be computed with a sum of contributions from all G energy groups as

$$f_i = \sum_{g=1}^G \nu \Sigma_f^{i,g} \overline{\phi_{i,g}} \quad (20)$$

for the current estimate of scalar fluxes $\overline{\phi_{i,g}}$. This can be used to evaluate the RMS fission rate error at iteration n as

$$\frac{1}{N_f} \sqrt{\sum_{i \in N_f} \left(\frac{f_i^n - f_i^{ref}}{f_i^{ref}} \right)^2} \quad (21)$$

where N_f is the number of regions with a nonzero neutron production rate, f_i^n refers to the neutron production rate of region i in iteration n , and f_i^{ref} represents the neutron production rates of a reference solution. This provides a reliable metric to evaluate convergence. However, it also requires knowledge of a reference solution, which is often unavailable. Therefore, the RMS iterative change in fission rate can be used as an alternative convergence metric, computed as

$$\frac{1}{N_f} \sqrt{\sum_{i \in N_f} \left(\frac{f_i^n - f_i^{n-1}}{f_i^{n-1}} \right)^2}. \quad (22)$$

In general, the RMS fission rate error is preferred since it better represents the deviation from the true solution in early iterations. Therefore, this study derives reference solutions from converging OpenMOC simulations on the same problem which are able to achieve a very small RMS iterative change in fission rate of 10^{-10} .

5. Simulation Models

5.1. The BEAVRS Benchmark

This study aims to demonstrate convergence behavior on realistic and relevant reactor physics models. Therefore, material and geometry definitions are taken from the BEAVRS benchmark [Horelik et al. \(2013\)](#) which was released in 2013, representing a Westinghouse 4-loop nuclear power reactor. This reactor is representative of common PWR designs in the United States. The reactor contains 193 fuel assemblies. Each assembly contains a 17×17 lattice of fuel rods, guide tubes, and instrument tubes. The pin-pitch is 1.26 cm inside each assembly. All fuel rods within the same assembly contain uranium of the same enrichment. This study focuses on the first cycle, which utilized three uranium enrichments: 1.6%, 2.4%, and 3.1%. A radial illustration of the BEAVRS benchmark is shown in Figure 2.

Using direct Monte Carlo simulation of the BEAVRS benchmark with the OpenMC code, reaction rate tallies are generated for each unique material. These allow for the computation of multi-group cross-sections using the `mgxs` package implemented by Boyd [Boyd \(2017\)](#). The Monte Carlo simulation used the JEFF-3.2 cross-section data at a temperature of 566.483K. 400 batches (300 inactive, 100 active) were simulated with 2×10^8 particles per batch to tally a 70 group cross-section library using the CASMO-4 energy group boundaries [Edenius et al. \(1995\)](#). The flux-limited transport correction is applied to the cross-sections using anisotropic scattering rate tallies [Yamamoto et al. \(2008\)](#).

A more complete description of the BEAVRS benchmark used in these trials and the multi-group cross-section can be found in [Gunow \(2018\)](#).

5.2. Single Assembly Model

While full core models are ideal for capturing realistic and relevant behavior, they are very computationally expensive for

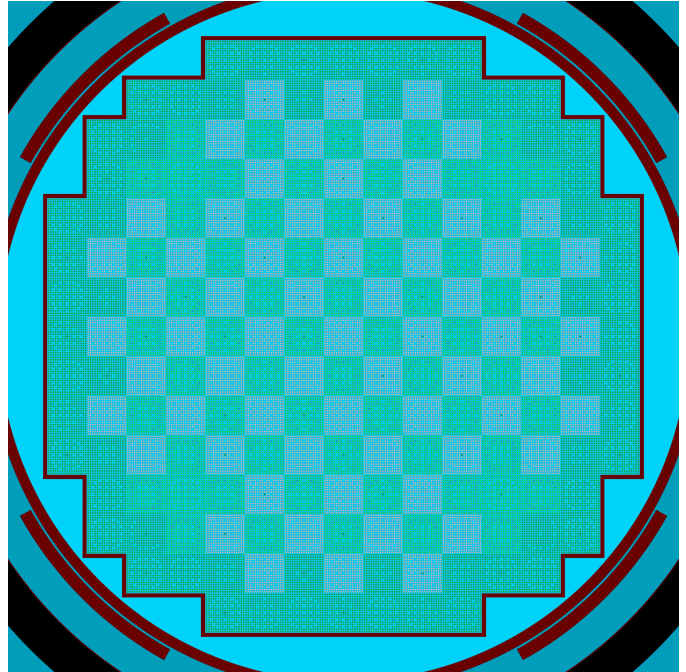


Figure 2. A radial view of the BEAVRS benchmark with regions colored by material.

3D neutron transport solvers, especially when extremely tight convergence is desired. Therefore, a single assembly model is formed which represents the full axial detail of a single 1.6% enriched fuel assembly. While this model lacks radial water reflectors, it contains the full axial detail of the full core problem, including grid spacers. Outside the core, full geometrical detail is also captured including support plate / nozzles and, most notably, water reflectors of approximately 20 cm above and below the fuel. Reflective boundaries are placed on the x and y boundaries and vacuum boundaries remain on the top and bottom of the model. A radial illustration of the single assembly model is shown in Figure 3.

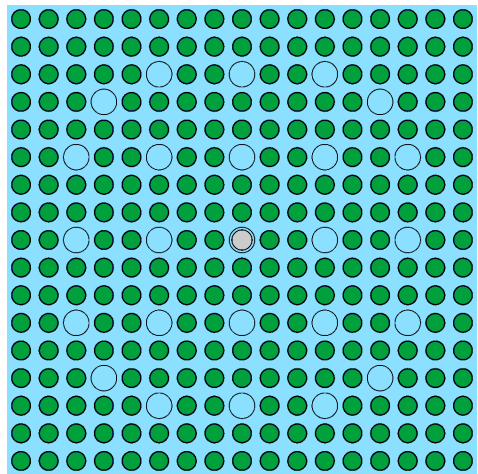


Figure 3. A radial view of the single assembly model with regions colored by material.

6. Results

6.1. MOC Parameters

The MOC parameters given in Table 1 are used for all tests presented in this study, unless noted otherwise. While finer MOC parameters would be necessary to accurately resolve the solution, refinements of the MOC parameters were observed to have little to no effect on the convergence behavior.

Table 1. MOC parameters for single assembly convergence studies

Source Approximation	Flat
Number of Sectors in Moderator	8
Number of Sectors in Fuel	4
Height of Flat Source Regions	2.0 cm
Radial Ray Spacing	0.1 cm
Axial Ray Spacing	1.5 cm
Number of Azimuthal Angles $\in [0, 2\pi]$	32
Number of Polar Angles $\in [0, \pi]$	6
Domain Decomposition	$1 \times 1 \times 100$

Note that spatial domain decomposition is implemented in OpenMOC [Gunow \(2018\)](#) and these single assembly tests were only domain decomposed in the axial direction (100 domains axially).

6.2. Convergence of Source Iteration

In order to focus on the asymptotic convergence behavior, rather than the behavior far from convergence, the MOC simulations start with a good guess of the scalar flux distribution. Specifically, the MOC convergence criteria is chosen to be extremely tight and a converging simulation where the error drops below 3×10^{-5} on RMS fission rate error is chosen as the starting point.

The convergence behavior is presented in Figure 4 in which the relative error is plotted as a function of iteration number for a variety of stabilizing schemes. Notice that the case without stabilization diverges while all the stabilization cases converge except for the diagonal stabilization scheme with insufficient damping (damping factor $\rho = 1/128$). This is expected since as ρ approaches zero, the stabilization method becomes equivalent to source iteration without stabilization. This clearly shows that this problem requires stabilization to converge with source iteration. In addition, the more conservative the stabilization scheme, the more convergence is slowed. The scheme proposed by Tabuchi slows convergence the most. The diagonal damping scheme hinders convergence significantly less, especially for $\rho < 1$.

7. Extension to Simulations with CMFD Acceleration

Often, CMFD acceleration is necessary to achieve reasonable convergence on practical reactor physics problems [Smith \(1983\)](#). The fundamental idea is that global information can be transferred much quicker over a coarse mesh than a fine mesh. Using this principle, CMFD acceleration alternates

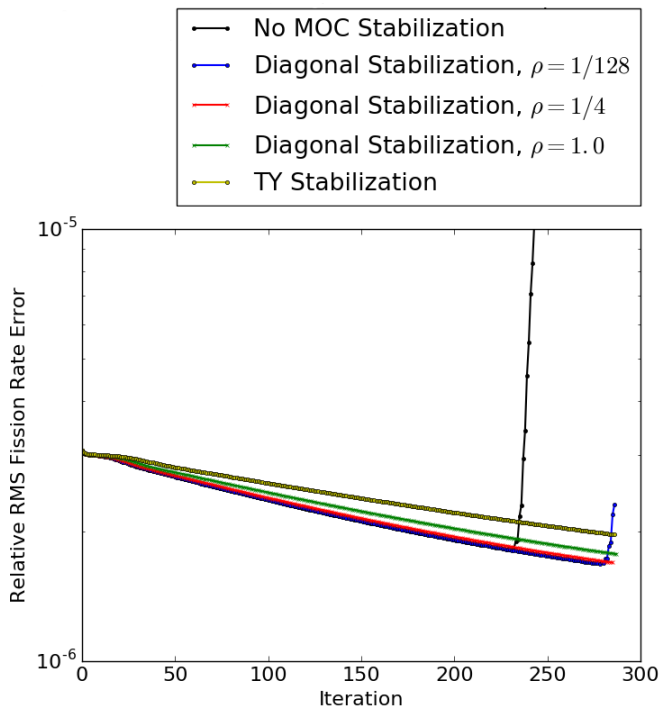


Figure 4. Convergence behavior of different stabilization schemes. TY Stabilization refers to the approach presented by Tabuchi whereas Diagonal Stabilization refers to the approach presented in this paper with damping coefficient ρ .

between solving a consistent set of diffusion equations on a coarse Cartesian mesh, where the model complexity is reduced and information propagates much quicker, and a fine mesh set of transport equations where the discretization accurately captures the solution of the problem.

The CMFD problem is computationally easier to solve than the transport equivalent due to the coarser mesh. In particular, a given CMFD cell j is comprised of many transport cells (MOC source regions) i . In order to make the CMFD problem even less computationally intense, the group structure can also be condensed. A group collapse is performed in which a given CMFD group e is formed from the incorporation of one or more transport groups g . To arrive at this relationship, the transport equation is summed over all transport groups g within the CMFD group e , shown in Eq. 23 with previously unidentified variable definitions presented in Table 2.

$$\sum_{g \in e} \left(\int_{S \in S_j} dS J_g(\mathbf{r}) \cdot \mathbf{n} + \sum_{i \in j} \Sigma_{tr}^{i,g} \overline{\phi_{i,g}} V_i \right) = \sum_{i \in j} \left(\frac{\sum_{g \in e} \chi_{i,g}}{k} \sum_{g'=1}^G \nu \Sigma_f^{i,g'} \overline{\phi_{i,g'}} V_i \right) + \sum_{g'=1}^G \left(\sum_{g \in e} \Sigma_s^{i,g' \rightarrow g} \right) \overline{\phi_{i,g'}} V_i \quad (23)$$

This equation can be re-written in terms of CMFD fluxes

Table 2. Variable definitions for Eq. 23

Variable	Definition
i	Transport Cell (MOC Source Region)
V_i	Volume of Cell i
j	CMFD Cell
S_j	Collection of Surfaces for Cell j
g	Transport Energy Group
e	CMFD Energy Group
\mathbf{r}	Position
\mathbf{J}_g	Net Current Vector for Group g
\mathbf{n}	Surface Normal Vector

and cross-sections, denoted with the subscript C , using the transport solution fluxes and cross-sections. The result is shown in Eq. 24, which assumes that all CMFD cells have exactly H surfaces.

$$\frac{1}{V_C} \sum_{h=1}^H \tilde{J}_{j,h,e} + \Sigma_{C,tr}^{j,e} \phi_C^{j,e} = \frac{\chi_C^{j,e}}{k} \sum_{e'=1}^E \nu \Sigma_{C,f}^{j,e'} \phi_C^{j,e'} + \sum_{e'=1}^E \Sigma_{C,s}^{i,e' \rightarrow e} \phi_C^{j,e'} \quad (24)$$

Note that this equation introduces the partial net current $\tilde{J}_{j,h,e}$ on surface h of CMFD cell j for CMFD group e , which is defined by

$$\frac{\tilde{J}_{j,h,e}}{A_{j,h}} = -u(j,h) \hat{D}_{j,e} (\phi_C^{I(j,h),e} - \phi_C^{j,e}) - \tilde{D}_{j,h,e} (\phi_C^{I(j,h),e} + \phi_C^{j,e}). \quad (25)$$

The function $u(j,h)$ is the *sense* of the surface h on cell j , $A_{j,h}$ is the area of surface $S_{j,h}$, $\hat{D}_{j,e}$ is the surface diffusion coefficient, the function $I(j,h)$ computes the index of the neighboring CMFD cell of j on surface h , and $\tilde{D}_{j,h,e}$ is the nonlinear corrected diffusion coefficient. The inspiration of the first term involving $\hat{D}_{j,e}$ comes from diffusion theory. Specifically it can be calculated using Eq. 26 under a CMFD uniform mesh assumption

$$\hat{D}_{j,h,e} = \frac{D_{j,e} D_{I(j,h),e}}{\Delta r_h (D_{j,e} + D_{I(j,h),e})} \quad (26)$$

where Δr_h is the distance between the CMFD cell and the interfacial surface h and $D_{j,e}$ is the diffusion coefficient of cell j in group e . Due to the uniform mesh assumption, the distance between the centroid of cell j and surface h is the same as that of the neighboring cell $I(j,h)$. In this study, the uniform mesh assumption is imposed, but a more general treatment is possible. The diffusion coefficients are defined in Eq. 27, with motivation from how diffusion coefficients are calculated in common nodal diffusion theory.

$$D_{j,e} = \frac{\sum_{i \in j} \sum_{g \in e} \frac{1}{3\Sigma_{tr}^{i,g}} \overline{\phi_{i,g}} V_i}{\sum_{i \in j} \sum_{g \in e} \overline{\phi_{i,g}} V_i} \quad (27)$$

Lastly, the corrected diffusion coefficients $\tilde{D}_{j,h,e}$ are computed based on the relationship in Eq. 25 for fluxes computed after the transport iteration and before the CMFD solve as

$$\tilde{D}_{j,h,e} = \frac{-u(j,h) \hat{D}_{j,h,e} (\tilde{\phi}_C^{I(j,h),e} - \tilde{\phi}_C^{j,e}) - \tilde{J}_{j,h,e}}{\tilde{\phi}_C^{I(j,h),e} + \tilde{\phi}_C^{j,e}} \quad (28)$$

where $\tilde{\phi}_C^{j,e}$ are the CMFD cell-averaged scalar fluxes calculated from the MOC iteration with the tilde indicating the quantity comes from the MOC calculation and does not change throughout the CMFD iterations. Note that this term is necessary to ensure consistency between the transport and CMFD equations. Often, a relaxation factor is applied to the corrected diffusion coefficients in order to ensure stability Smith and Rhodes (2002). With the relaxation factor ω , the computed corrected diffusion coefficients are damped in iteration $n+1$ by

$$\tilde{D}_{j,h,e}^{n+1} = \omega \tilde{D}_{j,h,e}^{n+1/2} + (1 - \omega) \tilde{D}_{j,h,e}^n \quad (29)$$

where the half-iterations refer to the computed diffusion coefficient without damping, as given in Eq. 28. The relaxation factor ω can be any real number in the interval $[0,1]$ chosen by the user. A lower relaxation factor leads to greater stability, but also leads to slower convergence.

After the CMFD solution is formed, it is used in a prolongation step to update the fluxes in the transport equation. Generally, this can be viewed as a non-linear operation f . Therefore, the iterative scheme with diagonal damping can be viewed as

$$\boldsymbol{\phi}_{n+1} = (I + D)^{-1} \left[f \left(J \left(\frac{1}{k} F + S \right) \boldsymbol{\phi}_n \right) + D \boldsymbol{\phi}_n \right] \quad (30)$$

where D is the diagonal stabilization matrix. Notice that diagonal stabilization is applied after prolongation, so it can still have a significant impact on convergence rate.

8. Convergence Results with CMFD Acceleration

In Section 6.2, the convergence of source iteration and its stability properties were discussed. When CMFD acceleration is applied, the behavior is much more difficult to analyze since CMFD is a non-linear process. Therefore, discussion of CMFD results will focus on hypotheses to explain the observed results rather than rigorous analysis.

In this section, the CMFD mesh is always chosen to be uniform with cells of pin-cell pitch in the radial dimensions and 2.0 cm in the axial dimension. All of the stability results presented in this section use the parameters in Section 1 with a CMFD relaxation factor of 0.7 unless otherwise specified. Many CMFD implementations choose to collapse to a fewer number of energy groups in order to improve the speed of the CMFD solver. While the CMFD equations are computationally less expensive in collapsed few-group structures, it is possible that collapsing group structures could cause slower convergence by not fully resolving spectral effects. Results with a variety of CMFD group structures are presented. While

the MOC calculation always uses a 70 group structure, CMFD group structures are formed with G_C CMFD groups, with group ranges taken from the CASMO-4 Manual [Edenius et al. \(1995\)](#).

8.1. Single Assembly Convergence with Water Reflectors

The single assembly model previously analyzed for pure source iteration in Section 6.2 is first analyzed with CMFD acceleration using the same parameters. It is important to remember that this problem includes axial water reflectors. These large regions of water where the transport-correction is large could potentially have a strong impact on convergence. The results with CMFD applied and *without* any MOC source iteration stabilization are shown in Figure 5 for a variety of CMFD group structures with the error once again relative to a tightly converged reference. As expected, most of the

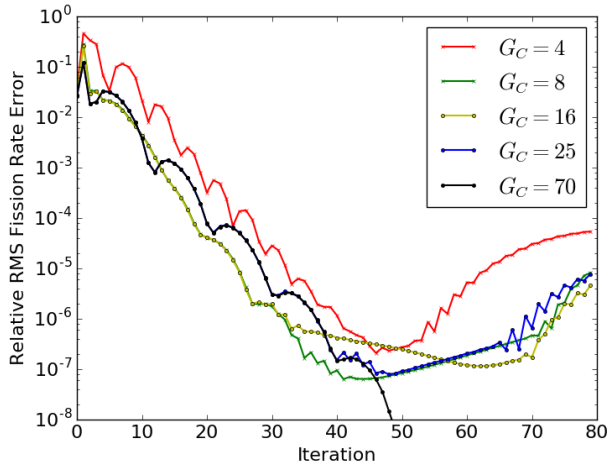


Figure 5. Convergence behavior for a variety of CMFD group structures with G_C CMFD groups and *without* MOC source iteration stabilization.

trials have trouble converging. This is likely due to the convergence issue observed with pure source iteration. However, the convergence with 70 group CMFD is stable. It is important to remember that the CMFD equations do not suffer from the issue of a negative dominant eigenvalue since the CMFD equations can be written such that within-group scattering does not arise when removal cross-sections are used instead of total cross-sections.

If 70 group CMFD is driving the convergence process, then the instability in the underlying source iteration technique is overcome by the CMFD acceleration prolongation in which MOC scalar fluxes are updated with the CMFD solution. One way of interpreting this behavior is to think of the convergence as being dominated by the CMFD acceleration where MOC transport sweeps are used purely to resolve local behavior, integrate reaction rates to form CMFD cross-sections, and tally currents crossing CMFD mesh surfaces.

However, with a reduced CMFD group structure, the flux distribution in energy within a single CMFD group *must* be resolved by the MOC source iteration process. Since the underlying MOC source iteration process is unstable, any reliance on

the process for convergence using a reduced group structure appears to lead to instability.

Since this convergence issue is fundamental, the process will eventually diverge if CMFD acceleration is turned off - even when the scalar fluxes are just a small deviation from the true solution (such as machine precision).

8.2. Single Assembly Convergence with Stabilization

To verify that the convergence issue can be remedied with MOC source iteration stabilization, the same single assembly test is conducted but using diagonal stabilization with $\rho = 1/4$. For pure source iteration, this was sufficient for stabilization, as previously shown in Figure 4. The results using this stabilization with CMFD acceleration are shown in Figure 6. As expected, the MOC source iteration stabilization

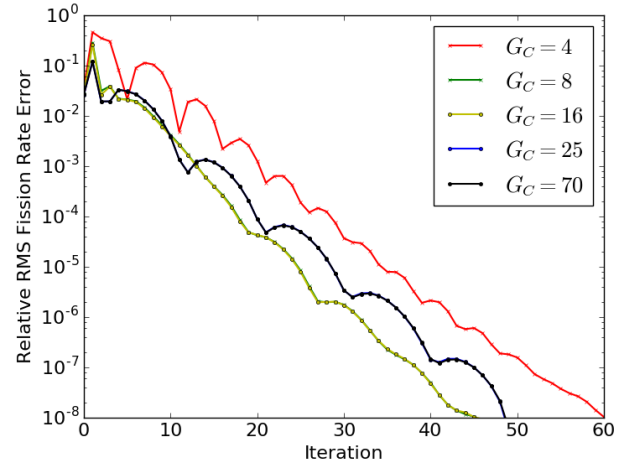


Figure 6. Convergence behavior for a variety of CMFD group structures with G_C CMFD groups and *with* Diagonal MOC source iteration stabilization ($\rho = 1/4$).

fixes the convergence issues for all CMFD group structures, indicating that the convergence issue was caused by the underlying MOC source iteration.

8.3. Single Assembly without Axial Water Reflectors

Next, a truncated single assembly model is studied. This model is the same as the single assembly model but without the axial water reflectors, with the entire axial extent of the model within the active fuel. A $1 \times 1 \times 90$ domain decomposition is used with domains of equal size as the single assembly model (20 cm height). Without reflectors, this model is similar to lattice physics models. The convergence behavior is analyzed *without* source iteration stabilization. The results with CMFD acceleration for a variety of CMFD group structures are presented in Figure 7. Notice that the convergence issues are not present in this model. This indicates the issue is caused by the axial water reflectors. More generally, it appears to be a problem with deep water reflectors that have negative cross-sections. Recall from the theory discussion that iteration matrix components in Eq. 9 were formed with the product of

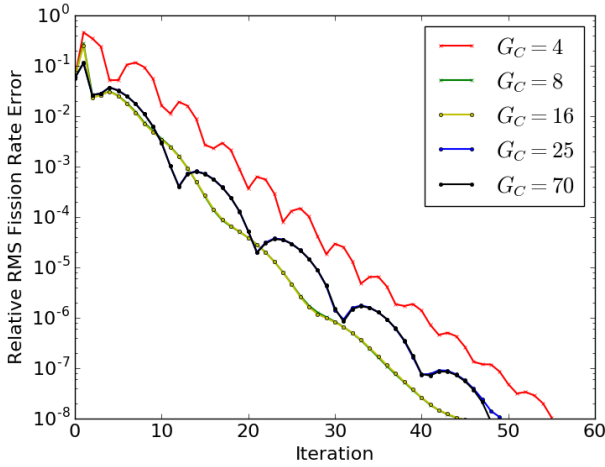


Figure 7. Convergence behavior for the single assembly *without* axial reflectors with a variety of CMFD group structures with G_C CMFD groups and *without* MOC source iteration stabilization.

collision probability and self-scattering cross-sections. In deep water reflectors, the probability of transport between water regions containing negative cross-sections is significantly higher than in the active fuel where many neutrons collide with fuel. This motivates neutron behavior in deep reflectors causing the instability.

9. Full Core Results

The previous results were focused on a single assembly with and without axial reflectors which proved the existence of source iteration instability. Since this issue seems to only appear at very low errors, the reader might judge this issue to be purely academic. However, for problems where deeper reflectors exist, such as a typical full core LWR problem, this issue is exacerbated. To test this effect, full core models are simulated using the same cross-section set applied in the single assembly studies. The geometry outside the core is radially discretized into a 3×3 square grid within each pin-cell-sized region.

9.1. 2D Extruded Model

Before simulating the explicit 3D model, a 2D extruded BEAVRS model is studied. This model lacks the axial water reflectors but still contains significant water reflectors in the radial direction. Specifically, a 10 cm tall cutout in active fuel (without any grid spacers) is simulated with reflective boundary conditions applied on the top and bottom. A $17 \times 17 \times 1$ domain decomposition is used. The results are shown in Figure 8. The simulation is run with 8 group and 70 group CMFD with Diagonal Stabilization. The damping coefficient ρ is chosen for both cases to be zero (equivalent to no stabilization) and $1/4$. For all reduced CMFD group structures, similar results are observed as seen with the 8 group CMFD structure in Figure 8 in which reasonable convergence can only be obtained by applying the MOC diagonal stabilization.

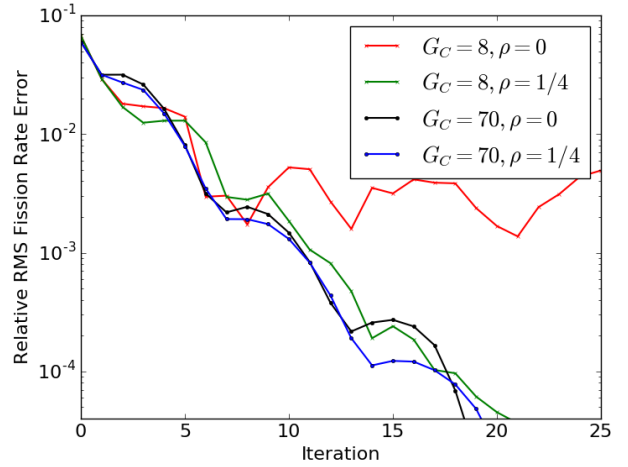


Figure 8. Convergence behavior of CMFD group structures with G_C CMFD groups and Diagonal MOC source iteration stabilization with stabilization coefficient ρ .

9.2. Explicit 3D Model

Now the full core 3D BEAVRS model is simulated. Since the problem is large, the MOC angular quadrature is significantly coarsened to 4 azimuthal angles and 2 polar angles in order to run a significant number of iterations on the Cetus partition of the Argonne BlueGene/Q supercomputer. These parameters are very coarse, but still exhibit the convergence issue. Since the run time with coarse angles can become dominated by the CMFD solution time, it is infeasible to use 70 CMFD groups on the Cetus partition. Therefore, results are presented only for a reduced 8 group CMFD structure. A $17 \times 17 \times 5$ domain decomposition is used. The results are shown in Figure 9 both with and without using the Diagonal Stabilization technique with $\rho = 1/4$.

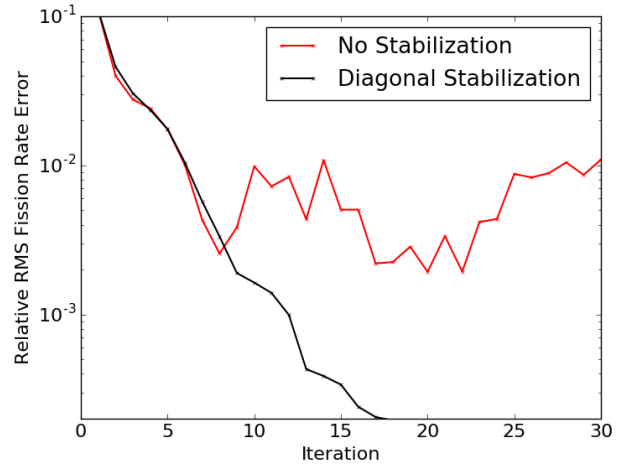


Figure 9. Convergence behavior of OpenMOC on the full core BEAVRS benchmark with and without Diagonal Stabilization ($\rho = 1/4$).

These results show that for the 3D full core PWR problem, a stabilization technique is necessary in order to reach any

reasonable convergence, especially when it is computationally infeasible to use a many-group CMFD solver.

10. Conclusion

In this study, a theoretical analysis of source iteration convergence was presented which showed the possibility for source iteration instabilities with transport-corrected cross-sections. The theory was broadened to include source iterations without within-group scattering iterations. A new diagonal stabilization technique was presented which is substantially less conservative than previously proposed techniques. Realistic reactor physics problems were presented that showed instability with the source iteration process. The diagonal stabilization technique was shown to successfully stabilize the source iteration process without having much impact on convergence rate.

Results were also presented for convergence with CMFD acceleration which showed that CMFD acceleration without group collapse was able to stabilize the source iteration process. For CMFD acceleration with a collapsed group structure, the previously discussed stabilization techniques were necessary to ensure convergence.

When the group structure is not collapsed in the CMFD solver, no convergence issues were observed. The CMFD equations can be converged since they do not rely on the source iteration technique. Due to their reduced dimensionality, the CMFD equations can be solved in explicit matrix form using a generic eigenvalue solver. It is inferred that the CMFD update has a larger impact on convergence than the update from each transport sweep, allowing CMFD acceleration to overcome the inherent source iteration instability by driving the convergence harder towards the physical solution than the transport sweeps drive towards nonphysical (negative eigenvalue) solutions. However, when the group structure is collapsed, the convergence depends on transport sweeps to resolve the energy spectrum within each CMFD energy group containing multiple transport energy groups. It is inferred that by relying on the transport sweeps to resolve the spectrum, the inherent instability in source iteration causes the process not to converge.

In the case of full core PWR problems, a collapsed group structure is often attractive to reduce run time, necessitating a stabilization method in order to converge. While the stabilization methods can cause slower convergence, the reduction in convergence rate was not very significant for the diagonal stabilization method, making it an attractive option for converging full core problems.

Acknowledgments

This work was supported in part by the Center for Exascale Simulation of Advanced Reactors (CESAR), a co-design center under the U.S. Department of Energy Contract No. DE-AC02-06CH11357. The first author was a recipient of the DOE Office of Nuclear Energy's Nuclear Energy University

Programs Fellowship. This research was performed, in part, using funding received from the DOE Office of Nuclear Energy's Nuclear Energy University Programs (contract number: DE-NE0008578). This research made use of the resources of the High Performance Computing Center at Idaho National Laboratory, which is supported by the Office of Nuclear Energy of the U.S. Department of Energy and the Nuclear Science User Facilities under Contract No. DE-AC07-05ID14517. Additionally, this research used resources of the Argonne Leadership Computing Facility, which is a DOE Office of Science User Facility supported under Contract DE-AC02-06CH11357.

References

- Bell, G., Hansen, G., Sandmeier, H., 1967. Multitable Treatments of Anisotropic Scattering in S N Multigroup Transport Calculations. Nuclear Science and Engineering 28 (3), 376–383.
- Boyd, W., et al., 2016. OpenMOC User's Guide – Theory and Methodology. <https://mit-crpg.github.io/OpenMOC/>, accessed: 2016-07-11.
- Boyd, W. R. D., 2017. Reactor agnostic multi-group cross section generation for fine-mesh deterministic neutron transport simulations. Ph.D. thesis, Massachusetts Institute of Technology.
- Bradie, B., 2006. A Friendly Introduction to Numerical Analysis. Pearson Prentice Hall, Upper Saddle River, New Jersey.
- Edenius, M., Ekberg, K., Forssén, B. H., Knott, D., 1995. CASMO-4, A Fuel Assembly Burnup Program, User's Manual. StudsvikOSA-9501, Studsvik of America, Inc.
- Ferrer, R., Rhodes, J., 1981. A Linear Source Approximation Scheme for the Method of Characteristics. Vol. 77. pp. 119–136.
- Ferrer, R., Rhodes, J., Smith, K., 2012. Linear Source Approximation in CASMO5. In: PHYSOR. Knoxville, TN, USA.
- Graham, A., 1987. Nonnegative Matrices and Applicable Topics in Linear Algebra. John Wiley & Sons.
- Gunow, G., Shaner, S., Forget, B., Smith, K., 2016. Reducing 3D MOC Storage Requirements with Axial On-the-fly Ray Tracing. In: PHYSOR 2016. Sun Valley, ID, USA.
- Gunow, G. A., 2018. Full core 3d neutron transport simulation using the method of characteristics with linear sources. Ph.D. thesis, Massachusetts Institute of Technology.
- Hansen, C., 1964. Numerical Methods of Reactor Analysis. Academic Press.
- Hébert, A., 2009. Applied Reactor Physics. Presses inter Polytechnique.
- Horelik, N., Herman, B., Forget, B., Smith, K., 2013. Benchmark for Evaluation and Validation of Reactor Simulations (BEAVRS), v1.0.1. In: Int. Conf. Math. and Comp. Methods Applied to Nuc. Sci. & Eng. Sun Valley, Idaho, USA.
- MacFarlane, R., 1993. TRANSX 2: A Code for interfacing MATXS Cross-Section Libraries to Nuclear Transport Codes. , Los Alamos National Laboratory.
- MacFarlane, R., 2000. PSR-480/NJOY99.0: Code System for Producing Pointwise and Multigroup Neutron and Photon Cross Sections from ENDF/B Data. , Los Alamos National Laboratory.
- Shaner, S., Gunow, G., Forget, B., Smith, K., 2015. Theoretical Analysis of Track Generation in 3D Method of Characteristics. In: International Conference on Mathematics and Computational Methods Applied to Nuclear Science and Engineering. Nashville, TN, USA.
- Smith, K. S., 1983. Nodal Method Storage Reduction by Non-linear Iteration. Vol. 44.
- Smith, K. S., Rhodes, J. D., 2002. Full-Core, 2-D, LWR Core Calculations with CASMO-4E. In: PHYSOR. Seoul, South Korea.
- Tabuchi, M., Tatsumi, M., Yamamoto, A., Endo, T., 2014. Improvement of a Convergence Technique for MOC Calculation with Large Negative Self-scattering Cross-section. In: PHYSOR. Kyoto, Japan.
- Tabuchi, M., Yamamoto, A., Endo, T., Sugimura, N., 2013. Convergence analysis of MOC inner iterations with large negative self-scattering cross-section. Journal of Nuclear Science and Technology 50 (5), 493–502.
- W. Boyd, S. Shaner, L. Li, B. Forget, and K. Smith, 2014. The OpenMOC Method of Characteristics Neutral Particle Transport Code. Annals of Nuclear Energy.

Yamamoto, A., Kitamura, Y., Yamane, Y., 2008. Simplified Treatments of Anisotropic Scattering in LWR Core Calculations. *Journal of Nuclear Science and Technology* 45 (3), 217–229.